Intrinsic anomalous Hall effect in altermagnets

Lotan Attias, ¹ Alex Levchenko, ² and Maxim Khodas, ¹ The Racah Institute of Physics, The Hebrew University of Jerusalem, Jerusalem 91904, Israel, ² Department of Physics, University of Wisconsin-Madison, Madison, Wisconsin 53706, USA

(Received 19 February 2024; revised 27 August 2024; accepted 3 September 2024; published 18 September 2024)

We study the anomalous Hall effect arising from the altermagnetic order and spin-orbit interaction in doped FeSb₂. To investigate the anomalous transport, we have constructed a tight-binding model of FeSb₂. We separately considered the constraints imposed on the model parameters by the spin symmetry group and magnetic symmetry group at zero and finite spin-orbit interaction, respectively. The resulting model includes the effect of exchange splitting and is applicable at both zero and finite spin-orbit interaction. In the case of spin symmetry, the analysis covers the spin-only subgroup arising from collinear magnetism, as well as nontrivial symmetry elements. This allows us to explore changes in the hopping amplitudes as symmetry is reduced by spin-orbit interaction from the spin group to the magnetic group. While the anomalous Hall effect is forbidden by spin symmetry, it is allowed by the symmetries of the magnetic group. The intrinsic Hall conductivity is shown to vanish linearly with spin-orbit interaction. This nonanalytic behavior is universal to altermagnets. It originates from the singularity of the Berry curvature localized along lines on a Fermi surface confined to symmetry planes. These planes host spin degeneracy protected by spin symmetry, which is lifted by spin-orbit interaction.

DOI: 10.1103/PhysRevB.110.094425

I. INTRODUCTION

Altermagnetism is a novel form of collinear magnetism, distinct from both ferromagnetism and antiferromagnetism [1–9]. For instance, in an altermagnet, zero net magnetization does not rule out a well-defined band spin polarization [10]. The latter arises from the combination of the antiferromagnetic order coupled to the itinerant spins and the nontrivial orbital wave function of the electronic states residing at the two magnetic sublattices, *A* and *B*.

The spin polarization in altermagnets is distinct from the more commonly known spin splitting induced by the spin-orbit interaction (SOI) in noncentrosymmetric materials. In the latter more familiar situation, the time-reversal symmetry (\mathcal{T}) is preserved while parity (\mathcal{P}) is broken. In contrast, in magnets \mathcal{T} is broken and the parity \mathcal{P} is often preserved.

When the antiferromagnetic order causes the doubling of a unit cell, the electronic bands remain spin degenerate. Indeed, in such cases even though \mathcal{T} is not a symmetry, the combination of \mathcal{T} and a translation ($\boldsymbol{\tau}$) that exchanges the magnetic sublattices is. As a result, spin states form the degenerate Kramers doublets related by the $\boldsymbol{\tau}\mathcal{T}\mathcal{P}$ antiunitary symmetry operation. Similarly, if the inversion \mathcal{P}' exchanging the A and B sublattices is a symmetry of the nonmagnetic crystal the two Kramers partners are related by $\mathcal{P}'\mathcal{T}$. In both scenarios no spin polarization of electronic bands arises.

In contrast, magnetic order of an altermagnet does not double the unit cell, and \mathcal{P}' is not a symmetry of the non-magnetic state. To form a symmetry \mathcal{T} has to be combined with some rotation. A given rotation R maps the generic electron momentum \mathbf{k} to another momentum $R\mathbf{k} \neq -\mathbf{k}$. As a consequence, a combined symmetry $R\mathcal{T}$ relates spin states at distinct momenta, $R\mathcal{T}\mathbf{k} \neq \mathbf{k}$, and therefore allows for a finite spin band splitting.

The above spin splitting may arise from a nontrivial magnetic form factor of localized magnetic moments [11–13]. Such moments are associated with the nonzero orbital angular momentum, l=2,4,6. The exchange interaction with these moments causes the spin splitting of itinerant electrons except for the ${\bf k}$ along the nodal directions of the magnetization density.

The spin splitting described above is a hallmark of altermagnetism. Clearly, it is unrelated to the SOI. Therefore, it arises most naturally in nonrelativistic density functional rheory (DFT) calculations, where the SOI is set to zero. The symmetry of a magnetic crystal at finite SOI is defined by the specific magnetic space group of a given crystal [14]. The symmetry operations in a magnetic space group act in the same way on positions of atomic sites and on the local magnetic moments. If, e.g., such transformation is a rotation it rotates both the crystal and magnetic moments.

At zero SOI, the system may possess symmetries that act differently on spin and orbital degrees of freedom [16]. In this case the symmetry operations form the so called spin (space) group containing the magnetic space group as a subgroup. For instance, in the case of the collinear magnetism considered here such group contains a trivial, and yet important, spin-only group. The latter contains an arbitrary angle rotation around the magnetization axis as well as rotation by π around an axis perpendicular to the magnetization axis followed by \mathcal{T} . The algorithm to construct all the possible spin groups for a given crystal and magnetic order has been formulated in Ref. [17].

Spin group symmetries protect extra spin degeneracies that appear as accidental from the point of view of a standard magnetic space group. An extended spin symmetry classification has been recently proposed to describe the spectrum degeneracies of collinear magnets in a nonrelativistic limit [18].

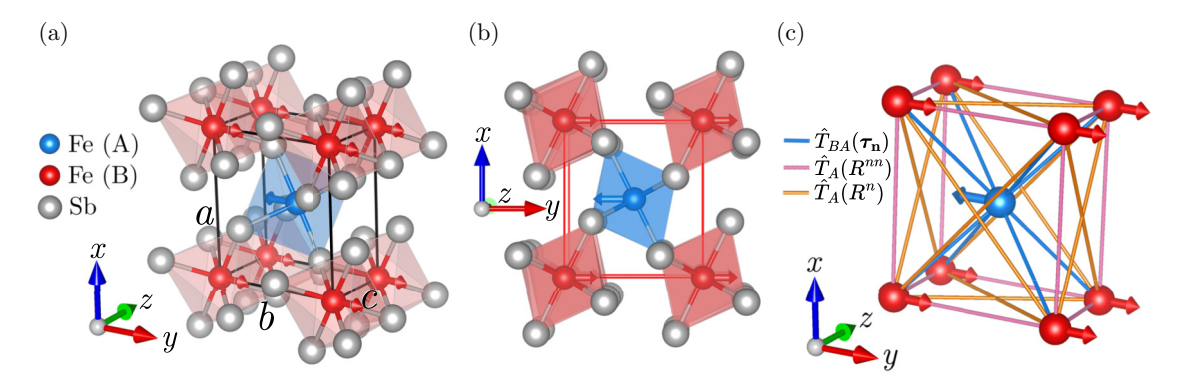


FIG. 1. Crystal structure of FeSb₂, space group 58. (a) Unit cell of FeSb₂ with the cages created by Sb atoms surrounding the Fe. The orthorhombic lattice distances along the \hat{x} , \hat{y} , \hat{z} directions are a, b, c. The two sublattices are oppositely polarized in the magnetic phase. (b) YZ-plane projection of FeSb₂. (c) Tight-binding hopping matrix elements for the intersublattice interaction, Eq. (9), and intrasublattice interactions, Eq. (23). The three amplitudes displayed define all other hopping matrix elements. Presentation is aided by VESTA [15].

The observation of robust anomalous Hall effect (AHE) in altermagnets such as RuO_2 [1,19] highlights the decisive role of the antiunitary symmetries in this class of magnets [20]. Here for definiteness, we focus on the FeSb₂ with an orthorhombic unit cell containing two distinct Fe atoms located at the A and B sublattices respectively. Fe atoms at the A and B sublattices are oppositely spin polarized along \hat{y} [see Figs. 1(a) and 1(b)].

The symmetry operations are outlined in Sec. II. In Sec. III we construct the minimal tight-binding model at zero and finite SOI. The AHE is studied in Sec. IV. We summarize in Sec. V.

II. SYMMETRIES AND BAND DEGENERACIES

In this section we introduce the magnetic space group Pnn'm' appropriate to $FeSb_2$ with finite SOI. We list the elements of the magnetic point group, $\mathcal{G}_M = G_M/\mathbf{R}$, which is a factor group of magnetic space group G_M by the group of translations, \mathbf{R} . \mathcal{G}_M contains unitary and antiunitary elements, and we employ the Wigner criterion to find out the momenta with double degeneracy due to antiunitary symmetries.

We then repeat the above steps for the spin group of antiferromagnetic $FeSb_2$ with zero SOI. The degeneracies have been studied in Ref. [10]. We rely on the results below as a consistency check. Moreover, it is of interest to apply the Wigner trichotomy test in a nonstandard setting of spin groups.

A. Finite SOI

In this case the magnetic point group can be presented as $\mathcal{G}_M = \mathcal{G}_M^u + \mathcal{T}C_{2z}\mathcal{G}_M^u$. Here the unitary elements form a simple Abelian subgroup, $\mathcal{G}_M^u = \{E, \mathcal{P}, \tau C_{2x}, \tau m_x\}$, where E is the identity operation and $m_x = \mathcal{P}C_{2x}$ is a mirror in the yz plane.

In the case of \mathcal{G}_M , the Wigner criterion states that for a given **k** one computes the sum to distinguish between the three cases:

$$\sum_{g \in \mathcal{G}_{M}^{u}}^{\prime} \chi^{\mathbf{k}}[(C_{2z}g)^{2}] = \begin{cases} +[\mathbf{k}]\mathcal{T}^{2} & \text{case (a)} \\ -[\mathbf{k}]\mathcal{T}^{2} & \text{case (b)}. \\ 0 & \text{case (c)} \end{cases}$$
(1)

In the case (a) the antiunitary operation $C_{2z}\mathcal{T}$ does not cause the extra degeneracy, and in cases (b) and (c) it does. The

band degeneracy, in addition, requires that there are elements $g \in \mathcal{G}_u$ such that $C_{2z}g$ reverses \mathbf{k} [21,22]. The summation in Eq. (1) runs over $[\mathbf{k}]$ such elements. The $\chi^{\mathbf{k}}$ is the irreducible character of the group of \mathbf{k} , $G_{\mathbf{k}}$.

Consider for illustration the generic point in the $k_y = \pi$ plane, $\mathbf{k} = (k_x, \pi, k_z)$. For generic k_x and k_z , the group $\mathcal{G}_{\mathbf{k}}$ contains only translations, \mathbf{R} . The sum in Eq. (1) reduces to a single term, $g = \tau C_{2x}$, $[\mathbf{k}] = 1$. And since this operation squares to $(C_{2z}\tau C_{2x})^2 = -\mathbf{R}_y C_{2y}^2$ with $\mathbf{R}_y = \hat{y}$, the sum in the Wigner criterion is trivially evaluated:

$$\chi^{\mathbf{k}}[(C_{2z}g)^2] = -\mathcal{T}^2.$$
 (2)

Indeed, $C_{2y}^2 = \mathcal{T}^2 = \mp 1$ for (half)-integer spin, and according to the Bloch theorem $\chi^{\mathbf{k}}(\mathbf{R}) = \exp(-i\mathbf{k}\mathbf{R})$. Based on Eq. (2) we conclude that the degeneracy of Bloch bands at the $k_y = \pi$ plane doubles due to the $C_{2z}\mathcal{T}$ antiunitary symmetry. Similar analysis shows that this statement holds true for two lines parallel to the \hat{y} axis, $(k_x = 0, k_z = \pi)$ and $(k_x = \pi, k_z = 0)$. In total, the subset with double degeneracy, \mathcal{K}_{SO} , included one plane and two lines.

B. Zero SOI

As discussed in Sec. I, this case requires an analysis of the spin group, G_S . Similar to magnetic groups, the spin point group $\mathcal{G}_S = G_S/\mathbf{R}$ contains the unitary elements \mathcal{G}_S^u as a subgroup of index 2:

$$\mathcal{G}_{S}^{u} = [(C_{\infty y}||E) + \tau C_{2x}(C_{\infty y}||E)] \times \{(E||E), (E||P), (E||m_{z}), (E||C_{2z})\},$$
(3)

where $g(g_s||g_o)$ denotes the operation with g_s (g_o) acting on spin (orbital) degrees of freedom, respectively, followed by the unitary or antiunitary operation g acting in the same way on both degrees of freedom. Operations $(C_{\infty y}||E)$ form a unitary subgroup of the spin-only group, $(C_{\infty y}||E) + \mathcal{T}(C_{2x}||E)(C_{\infty y}||E)$, acting only on spins [17]. It emerges as spins decoupled from the orbital motion can be freely rotated around the magnetization axis by an arbitrary angle without affecting the Hamiltonian. The second line of Eq. (3) reflects the C_{2h} site symmetry of the Sb cage enclosing Fe atoms at both sublattices.

TABLE I. The action of the orbital part of the operations from the list $C_{2x}\{E, \mathcal{P}, m_z, C_{2z}\}$ on the momentum $\mathbf{k} = (k_x, k_y, k_z)$.

C_{2x}	$m_{\scriptscriptstyle X}$	$m_{\rm y}$	C_{2y}
$(k_x, -k_y, -k_z)$	$(-k_x, k_y, k_z)$	$(k_x, -k_y, k_z)$	$(-k_x, k_y, -k_z)$

The full spin point group including the antiunitary operations can then be represented in a compact form as

$$\mathcal{G}_S = \mathcal{G}_S^u + \tau \mathcal{T}(E||C_{2x})\mathcal{G}_S^u. \tag{4}$$

Before considering the possible doubling of the degeneracy due to nonunitary symmetries, one has to determine the irreducible representation of the group of \mathbf{k} , $G_{\mathbf{k}}$. The elements acting on the orbital degrees of freedom form a D_{2h} Abelian group. This allows us to focus on spin degeneracy.

At a generic **k**, up to translations, $G_{\mathbf{k}} = (C_{\infty y}||E)$ and the irreducible representations are one dimensional. Hence there is no spin degeneracy unless **k** is invariant under one of the four operations, $C_{2x}\{E, \mathcal{P}, m_z, C_{2z}\}$. These operations are listed in Table I along with their action on **k**. It follows directly from Table I that the spin degeneracy is doubled at four planes $k_x = 0$, π and $k_y = 0$, π comprising the set \mathcal{K}_{alt} . For instance, the $k_y = \pi$ plane is invariant under $C_{2x}m_z = m_y$ operation.

In contrast to the magnetic group, the antiunitary operations of the spin group do not lead to degeneracy doubling. We demonstrate this by extending the Wigner criterion to the spin group (see Appendix A for details).

III. SINGLE ORBITAL TIGHT-BINDING MODEL

We construct the tight-binding model of itinerant electrons to incorporate the SOI and the exchange coupling in an altermagnet. We start with the atomic limit by looking at the effect of the lattice on electronic states localized at a given lattice site. The exchange splitting $2B_{\rm ex}$ is assumed to be much larger than the spin splitting induced by the SOI locally at a given site. This makes it reasonable to ignore the local effect of SOI. In contrast, we do study in detail the effect of SOI on the hopping amplitudes to the neighboring sites in the following sections.

In the absence of the local SOI, the spin and orbital degrees of freedom at each site decouple. We therefore, discuss the localized orbital wave functions ignoring the spin. The site symmetry group is Abelian, and the Sb cage lifts the orbital degeneracy at Fe sites. Hence, we focus on a single orbital model with orbital wave functions $\phi_{A(B)}(\mathbf{r})$ at the A and B sublattices.

The nonsymmorphic τC_{2x} symmetry implies the relationship $\phi_B(\mathbf{r}) = \phi_A(C_{2x}^{-1}\mathbf{r})$. It is crucial for altermagnetism that the functional forms of the $\phi_A(\mathbf{r})$ and $\phi_B(\mathbf{r})$ orbital wave functions of the two members in each degenerate doublet may differ. Indeed the on-site symmetry allows orbitals of same parity that are both even or odd with respect to C_{2z} to hybridize. This makes room for the hybridization of orbitals transforming differently under C_{2x} . For instance, the hybridization of s and d_{xy} orbitals gives rise to distinct orbital wave functions at the two sublattices [see Fig. 2(a)]. This point is further elaborated upon in Sec. III B.

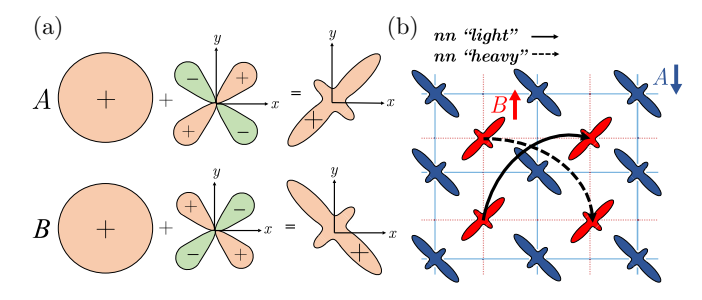


FIG. 2. (a) Symmetry-allowed hybridization of s and d_{xy} orbitals at Fe sites. The hybridized wave functions at the A and B sublattices are related by the nonsymmorphic τC_{2x} symmetry operation. As a result, the hybridized orbital wave functions at the two sublattices are distinct. (b) The projection of the crystal structure on the xy plane. The difference in the orbital wave functions for the two sublattices implies $A' \neq 0$ in Eq. (25) causing a spin splitting even at zero SOI.

These considerations naturally lead us to the tight-binding four band model

$$\mathcal{H} = \sum_{\mathbf{k}} \Psi_{\mathbf{k}\alpha}^{\dagger} \hat{H}_{\alpha\beta}(\mathbf{k}) \Psi_{\mathbf{k}\beta} \tag{5}$$

expressed in terms of the generalized Nambu spinor:

$$\Psi_{\mathbf{k}}^{\dagger} = [\psi_{\mathbf{k}A\uparrow}^{\dagger}, \psi_{\mathbf{k}A\downarrow}^{\dagger}, \psi_{\mathbf{k}B\uparrow}^{\dagger}, \psi_{\mathbf{k}B\downarrow}^{\dagger}]. \tag{6}$$

When applied to vacuum, $|0\rangle$, $\psi_{\mathbf{k}As}^{\dagger}$, and $\psi_{\mathbf{k}Bs}^{\dagger}$ create the electronic Bloch states localized at the A and B sublattices, respectively, with two possible spin projections on the \hat{z} axis. Specifically,

$$\psi_{\mathbf{k}As}^{\dagger}|0\rangle = \frac{1}{\sqrt{N}} \sum_{\mathbf{R} \in A} e^{i\mathbf{k}\mathbf{R}} \phi_A(\mathbf{r} - \mathbf{R}) \chi_s,$$
 (7a)

$$\psi_{\mathbf{k}Bs}^{\dagger}|0\rangle = \frac{1}{\sqrt{N}} \sum_{\mathbf{R} \in A} e^{i\mathbf{k}(\mathbf{R}+\mathbf{\tau})} \phi_B(\mathbf{r} - \mathbf{R} - \mathbf{\tau}) \chi_s,$$
 (7b)

where N Fe ions of the A sublattice are located at the sites of the orthorhombic lattice, $\mathbf{R} = n_x a \hat{x} + n_y b \hat{y} + n_z c \hat{z}$, defined by the vector $\mathbf{n} = (n_x, n_y, n_z)$ with integer valued components [see Fig. 1(a)]. Hereinafter, the distances along the three crystallographic directions are measured in units of a, b, and c, respectively. Correspondingly, the momentum components k_x , k_y , and k_z are measured in units of a^{-1} , b^{-1} , and c^{-1} .

To parametrize the Hamiltonian (5) we introduce the two sets of Pauli matrices, \varkappa and σ , acting in sublattice and spin spaces, respectively. The unit matrices acting in these spaces are denoted as \varkappa_0 and σ_0 . The generic model Hamiltonian reads

$$\hat{H}(\mathbf{k}) = \hat{H}^{e}(\mathbf{k}) + \hat{H}_{n}^{a}(\mathbf{k}) + \hat{H}_{nn}^{a}(\mathbf{k}) + \hat{H}_{ex}(\mathbf{k}), \tag{8}$$

where the exchange interaction is $\hat{H}_{ex} = B_{ex} \varkappa_z \sigma_y$, $\hat{H}^e(\mathbf{k})$ is the contribution of the nearest neighbor intersublattice hopping processes, and $\hat{H}_n^a(\mathbf{k})$ and $\hat{H}_{nn}^a(\mathbf{k})$ originate from the nearest and next to nearest neighbor intrasublattice hopping processes, respectively. Below we obtain the generic form of these terms constrained by the \mathcal{G}_M and \mathcal{G}_S symmetries.

A. Nearest neighbor intersublattice hopping processes

We start with the analysis of the $\hat{H}^e(\mathbf{k})$ part of the tight-binding Hamiltonian. The real space hopping matrix elements

TABLE II. The nearest neighbor intersublattice hopping parameters constrained by Eq. (16). The four out of eight hopping vectors, $\tau_n = n/2$, are sufficient in view of Eq. (13), and $\tau_{-n} = -\tau_n$. The Bravais lattice vector, $\Delta R(\tau_n)$, is introduced in Eq. (12). For the neighboring sites that are not shown it is given by $\Delta R(-\tau_n) = -\hat{x} - \hat{y} - \hat{z} - \Delta R(\tau_n)$. These parameters are visualized in Fig. 5(a) of Appendix B.

n	(1,1,1)	(-1, 1, 1)	(1, -1, 1)	(1, 1, -1)
$t_0(\boldsymbol{\tau_n})$	t_0	t_0^*	t_0	t_0^*
$t_{x}(\boldsymbol{\tau}_{\mathbf{n}})$	$t_{\scriptscriptstyle X}$	t_x^*	t_x	t_x^*
$t_{y}(\boldsymbol{\tau}_{\mathbf{n}})$	t_y	$-t_{v}^{*}$	$-t_y$	t_{v}^{*}
$t_z(\boldsymbol{\tau_n})$	t_z	$-t_z^*$	t_z	$-t_z^*$
$\Delta R(\tau_n)$	0	$-\hat{x}$	$-\hat{y}$	$-\hat{z}$

of the full microscopic space periodic Hamiltonian H are introduced in a standard way:

$$T_{BA}^{s's}(\tau_{\mathbf{n}}) = \langle \phi_B(\mathbf{r} - \tau_{\mathbf{n}}) \chi_{s'} | H | \phi_A(\mathbf{r}) \chi_s \rangle. \tag{9}$$

A given A site has eight neighboring sites to hop to in the B sublattice with the hopping vectors $\tau_{\mathbf{n}} = (1/2)(n_x\hat{x} + n_y\hat{y} + n_z\hat{z})$ fixed by the choice of $n_{x,y,z} = \pm 1$ [see Fig. 1(c)]. In particular, $\tau_{\mathbf{n}} = \tau$ for $n_x = n_y = n_z = 1$. It is convenient to represent the spin dependence of amplitude Eq. (9) in the form

$$\hat{T}_{BA}(\boldsymbol{\tau}_{\mathbf{n}}) = \sum_{\mu} t_{\mu}(\boldsymbol{\tau}_{\mathbf{n}}) \sigma_{\mu}, \tag{10}$$

where μ runs over the four values 0, x, y, and z.

The tight-binding Hamiltonian resulting from the intersublattice hopping processes reads

$$\hat{H}_e(\mathbf{k}) = \sum_{\mu} \left[\varkappa_x t_{\mu}^R(\mathbf{k}) + \varkappa_y t_{\mu}^I(\mathbf{k}) \right] \sigma_{\mu}, \tag{11}$$

where $t_{\mu}^{R}(\mathbf{k})$ and $t_{\mu}^{I}(\mathbf{k})$ are real and imaginary parts of

$$t_{\mu}(\mathbf{k}) = \sum_{\tau_{\mathbf{n}}} e^{-i\mathbf{k}[\Delta \mathbf{R}(\tau_{\mathbf{n}}) + \tau]} t_{\mu}(\tau_{\mathbf{n}}). \tag{12}$$

Here $\Delta \mathbf{R}(\tau_n)$ is the Bravais lattice vector connecting the unit cells hosting the neighboring sites at A and B sublattices (see Table II).

1. Finite SOI

We now turn to the constraints imposed on the matrix elements Eq. (9) by the magnetic point group, \mathcal{G}_M . The parity \mathcal{P} imposes the condition

$$\hat{T}_{RA}(\boldsymbol{\tau}_{\mathbf{n}}) = \hat{T}_{RA}(-\boldsymbol{\tau}_{\mathbf{n}}). \tag{13}$$

The unitary symmetry τC_{2x} imposes the constraint

$$\hat{T}_{BA}(\boldsymbol{\tau}_{\mathbf{n}}) = \sigma_{x} [\hat{T}_{BA}(C_{2x}\boldsymbol{\tau}_{\mathbf{n}})]^{\dagger} \sigma_{x}. \tag{14}$$

The antiunitary symmetry $C_{2r}\mathcal{T}$ leads to the condition

$$\hat{T}_{BA}(\boldsymbol{\tau}_{\mathbf{n}}) = \sigma_{\boldsymbol{x}} [\hat{T}_{BA}(C_{2\boldsymbol{z}}\boldsymbol{\tau}_{\mathbf{n}})]^* \sigma_{\boldsymbol{x}}. \tag{15}$$

Applying the set of Eqs. (13), (14), and (15) to Eq. (10) yields the following constraints:

$$t_{0(x)}(\boldsymbol{\tau}_{\mathbf{n}}) = t_{0(x)}(-\boldsymbol{\tau}_{\mathbf{n}}) = t_{0(x)}^{*}(C_{2x}\boldsymbol{\tau}_{\mathbf{n}}) = t_{0(x)}^{*}(C_{2z}\boldsymbol{\tau}_{\mathbf{n}}),$$
 (16a)

$$t_{v}(\tau_{\mathbf{n}}) = t_{v}(-\tau_{\mathbf{n}}) = -t_{v}^{*}(C_{2x}\tau_{\mathbf{n}}) = t_{v}^{*}(C_{2z}\tau_{\mathbf{n}}),$$
 (16b)

$$t_z(\tau_{\mathbf{n}}) = t_z(-\tau_{\mathbf{n}}) = -t_z^*(C_{2x}\tau_{\mathbf{n}}) = -t_z^*(C_{2z}\tau_{\mathbf{n}}).$$
 (16c)

Equation (16) implies that \mathcal{G}_M reduces the 32 complex parameters in Eq. (9) down to four, $t_\mu = t_\mu(\tau)$. The eight real parameters fixing the Hamiltonian Eq. (11) are the real and imaginary parts, t_μ^R and t_μ^I of t_μ . The rest of the hopping amplitudes follow from Eq. (16) as summarized in Table II. It turns out to be convenient to split the resulting tight-binding Hamiltonian Eq. (11) into two parts, $\hat{H}^e(\mathbf{k}) = \hat{H}^e_{\mathcal{T}}(\mathbf{k}) + \hat{H}^e_{\mathrm{B}}(\mathbf{k})$, where the first part $\hat{H}^e_{\mathcal{T}}(\mathbf{k})$ is invariant under \mathcal{T} , and the second part $\hat{H}^e_{\mathrm{B}}(\mathbf{k})$ breaks \mathcal{T} and is associated, therefore, with the exchange field, \mathbf{B} . We have

$$\hat{H}_{\mathcal{T}}^{e}(\mathbf{k}) = 8t_{0}^{R} \varkappa_{x} \sigma_{0} \cos \frac{k_{x}}{2} \cos \frac{k_{y}}{2} \cos \frac{k_{z}}{2}$$

$$-8t_{x}^{I} \varkappa_{y} \sigma_{x} \sin \frac{k_{x}}{2} \cos \frac{k_{y}}{2} \sin \frac{k_{z}}{2}$$

$$-8t_{y}^{I} \varkappa_{y} \sigma_{y} \cos \frac{k_{x}}{2} \sin \frac{k_{y}}{2} \sin \frac{k_{z}}{2}$$

$$+8t_{z}^{I} \varkappa_{y} \sigma_{z} \cos \frac{k_{x}}{2} \cos \frac{k_{y}}{2} \cos \frac{k_{z}}{2}, \qquad (17)$$

and the terms induced by the exchange field:

$$\hat{H}_{B}^{e}(\mathbf{k}) = -8t_{0}^{I} \varkappa_{y} \sigma_{0} \sin \frac{k_{x}}{2} \cos \frac{k_{y}}{2} \sin \frac{k_{z}}{2}$$

$$\times 8t_{x}^{R} \varkappa_{x} \sigma_{x} \cos \frac{k_{x}}{2} \cos \frac{k_{y}}{2} \cos \frac{k_{z}}{2}$$

$$-8t_{y}^{R} \varkappa_{x} \sigma_{y} \sin \frac{k_{x}}{2} \sin \frac{k_{y}}{2} \cos \frac{k_{z}}{2}$$

$$-8t_{z}^{R} \varkappa_{x} \sigma_{z} \sin \frac{k_{x}}{2} \cos \frac{k_{y}}{2} \sin \frac{k_{z}}{2}.$$
(18)

The spectrum of both Eqs. (17) and (18) taken separately is Kramers degenerate. In the case of Eq. (17) this is due to the combined TP symmetry. In the case of Eq. (18) it occurs because of the $\varkappa_z TP$ thanks to the chiral symmetry \varkappa_z characteristic for the intersublattice processes on a bipartite lattice.

The terms respecting \mathcal{T} symmetry, Eq. (17), are obtained when the exchange field breaking \mathcal{T} is set to zero. They, therefore, give the usual SOI, and as expected agree with the results of Ref. [23], where the \mathcal{T} -breaking term describing the coupling to the exchange field is added separately.

In contrast, the terms breaking \mathcal{T} symmetry, Eq. (18), require a finite **B**. Some of these terms result from the combined action of the SOI and the exchange field. Still, others are independent of SOI. The framework of the spin symmetries allows one to disentangle these two spin dependent interactions. And that is what we do next.

2. Zero SOI

Since the magnetic group \mathcal{G}_M is the subgroup of the spin group, \mathcal{G}_S , Eqs. (17) and (18) still hold, possibly with some of the coefficients forced to be zero due to a larger spin symmetry group. The spin-only group implies that all the terms in $\hat{H}_e(\mathbf{k})$ proportional to σ_x or σ_z are zero. In particular, we have $t_x^{R,I} = t_z^{R,I} = 0$ in Eqs. (17) and (18). This conclusion is quite obvious given that the magnetism in the case of zero SOI is collinear.

The less obvious conclusions are obtained as one considers nontrivial spin group operations. The $(E||m_\tau)$ operation acting

on orbital degrees of freedom implies

$$\hat{T}_{RA}(\boldsymbol{\tau}_{\mathbf{n}}) = \hat{T}_{RA}(m_z \boldsymbol{\tau}_{\mathbf{n}}), \tag{19}$$

which upon comparison with Table II yields $t_0 = t_0^*$ and $t_y = t_y^*$. The nonunitary symmetry $\tau \mathcal{T}(E||C_{2x})$ yields the constraint

$$\hat{T}_{BA}(\boldsymbol{\tau}_{\mathbf{n}}) = \sigma_{\mathbf{y}} \hat{T}_{BA}^{tr}(C_{2x}\boldsymbol{\tau}_{\mathbf{n}}) \sigma_{\mathbf{y}}. \tag{20}$$

This condition does not constrain $\hat{H}_e(\mathbf{k})$ farther.

The rest of the operations beyond the spin-only group are obtained by combining the operations considered so far with \mathcal{G}_M , and therefore do not result in additional constraints. As a consistency check we may consider the operation $\mathcal{T}(C_{2x}||E) = (\tau C_{2x})\tau \mathcal{T}(E||C_{2x})$. It implies

$$\hat{T}_{BA}(\boldsymbol{\tau}_{\mathbf{n}}) = \sigma_{z} [\hat{T}_{BA}(\boldsymbol{\tau}_{\mathbf{n}})]^{*} \sigma_{z}. \tag{21}$$

And again, $t_0^I = t_x^I = 0$. As expected, it contains no new information. In summary, at zero SOI and finite exchange field, the intersublattice hopping Hamiltonian takes the form

$$\hat{H}^{e}(\mathbf{k}) = 8t_{0}^{R} \varkappa_{x} \sigma_{0} \cos \frac{k_{x}}{2} \cos \frac{k_{y}}{2} \cos \frac{k_{z}}{2}$$
$$-8t_{y}^{R} \varkappa_{x} \sigma_{y} \sin \frac{k_{x}}{2} \sin \frac{k_{y}}{2} \cos \frac{k_{z}}{2}. \tag{22}$$

Here the first term is the usual spin independent contribution to the dispersion. The second term is the spin dependent contribution arising ultimately from the exchange interaction. Although this term is similar in form to the SOI, it is fundamentally distinct from it. It breaks $\mathcal T$ and exists at zero SOI interaction.

B. Intrasublattice hopping processes

We now turn to the intrasublattice part of the tight-binding Hamiltonian, $\hat{H}^a(\mathbf{k})$. Since the spin dependence has been considered in detail in Sec. III A, here we focus on the spin independent part of the tight-binding Hamiltonian. As we will see, the generic Hamiltonian describes hopping processes into nearest and next to nearest neighboring sites. The hopping amplitudes for these processes are defined similarly to Eq. (9):

$$T_A(\mathbf{R}^{n(nn)}) = \frac{1}{2} \sum_{s} \langle \phi_A(\mathbf{r} - \mathbf{R}^{n(nn)}) \chi_s | H | \phi_A(\mathbf{r}) \chi_s \rangle, \quad (23)$$

where \mathbf{R}^n and \mathbf{R}^{nn} denote the vectors connecting nearest and next to nearest neighbors on the A sublattice. The same definition is adopted for $T_B(\mathbf{R}^{n(m)})$ for the hopping amplitude on the B sublattice. The vector \mathbf{R}^n can take six values: $\pm \hat{x}$, $\pm \hat{y}$, and $\pm \hat{z}$. The vector \mathbf{R}^{nn} can take 12 values: $\pm \hat{x}$, $\pm \hat{y}$, $\pm \hat{z}$, $m_1\hat{x} + m_2\hat{y}$, $m_1\hat{y} + m_2\hat{z}$, and $m_1\hat{x} + m_2\hat{z}$ for $m_{1,2} = \pm 1$.

Consider first the nearest neighbor hopping amplitudes, $\hat{H}_n^a(\mathbf{k})$. Both at finite and zero SOI, the symmetry constrains it to be the same for the two sublattices:

$$\hat{H}_n^a(\mathbf{k}) = \varkappa_0 \sigma_0 [A_0 + f_1(\mathbf{k})],$$

$$f_1(\mathbf{k}) = A_x \cos k_x + A_y \cos k_y + A_z \cos k_z, \tag{24}$$

where A_0 , A_x , A_y , and A_z are three real parameters.

Qualitatively, we expect a sublattice dependence at the level of the next to nearest neighbors [see Fig. 2(b)]. In this

TABLE III. The next nearest neighbor intrasublattice hopping parameters constrained by the symmetry. The six out of twelve amplitudes are shown. The rest follows from the symmetry of all the amplitudes under reversal of $\Delta \mathbf{R}$. These parameters are visualized in Fig. 5(b) of Appendix B.

$\Delta \mathbf{R}$	$\hat{x} + \hat{y}$	$\hat{x} - \hat{y}$	$\hat{y} + \hat{z}$	$\hat{y} - \hat{z}$	$\hat{z} + \hat{x}$	$\hat{z} - \hat{x}$
$T_A(\Delta \mathbf{R})$ $T_B(\Delta \mathbf{R})$	$A_+ \ A$	$A \ A_+$	A_1 A_1	A_1 A_1	A_2 A_2	A_2 A_2

case the symmetry reduces the 24 real parameters down to four (see Table III). Notably, $T_A(\hat{x} \pm \hat{y}) = A_{\mp}$ and $T_B(\hat{x} \pm \hat{y}) = A_{\pm}$, with all the rest of the amplitudes being equal on the two sublattices. The feature essential for the altermagnetism is $A_+ \neq A_-$. Since $\hat{H}_{nn}^a(\mathbf{k})$ is generally weaker than $\hat{H}_n^a(\mathbf{k})$ it is permissible to retain only the essential part of $\hat{H}_{nn}^a(\mathbf{k})$ by setting $A_+ = -A_- = A'$, and the rest of the amplitudes to zero:

$$\hat{H}_{nn}^{a}(\mathbf{k}) = 2A' \varkappa_{z} \sigma_{0} f_{2}(\mathbf{k}), \quad f_{2}(\mathbf{k}) = 2 \sin k_{x} \sin k_{y}. \quad (25)$$

Qualitatively, the emergence of a finite spin splitting at zero SOI can be understood as originating from the difference in the orbital wave function for the two sublattices as shown in Fig. 2(b). We note, however, that even if such difference is not included, the finite A' in Eq. (25) results from the sublattice dependent potential experienced by an electron hopping to the next to nearest neighbors in the xy plane. Indeed, this has been found in Ref. [23] for a model with identical $d_{x^2-y^2}$ orbital wave functions on the two sublattices. In fact, these are the two manifestations of the same sublattice asymmetry.

C. Band degeneracies of the model Hamiltonian

Here we discuss the band degeneracies of the model Hamiltonian, Eq. (8), and compare them with the general results of Sec. II.

1. Nonzero SOI

In this case the Hamiltonian, Eq. (8), is given by Eqs. (17), (18), (24), and (25). We have confirmed the double degeneracy at $\mathbf{k} \in \mathcal{K}_{SO}$.

2. Zero SOI

To study the spectrum degeneracies it is enough to consider the difference, $\Delta \hat{H}(\mathbf{k}) = \hat{H}(\mathbf{k}) - \hat{H}_n^a(\mathbf{k})$, as the term $\hat{H}_n^a(\mathbf{k}) \propto \varkappa_0 \sigma_0$, Eq. (24). According to Eq. (22), the spin along the magnetization is a good quantum number, and the spectrum splits into two bands $\Delta \hat{H}_{\pm}$ for the two spin wave functions $\bar{\chi}_{\pm} = (\chi_{\uparrow} \pm i \chi_{\downarrow})/\sqrt{2}$ satisfying $\sigma_{\nu} \bar{\chi}_{\pm} = \pm \bar{\chi}_{\pm}$:

$$\Delta \hat{H}_{\pm}(\mathbf{k}) = \pm B_{\text{ex}} \varkappa_z + 2A' \varkappa_z f_2(\mathbf{k})$$

$$+ 8t_0^R \varkappa_x \cos \frac{k_x}{2} \cos \frac{k_y}{2} \cos \frac{k_z}{2}$$

$$\mp 8t_y^R \varkappa_x \sin \frac{k_x}{2} \sin \frac{k_y}{2} \cos \frac{k_z}{2}.$$
(26)

The eigenvalues E_{\pm} of $\Delta \hat{H}_{\pm}$ satisfy

$$E_{\pm}^{2} = [B_{\text{ex}} \pm 2A' f_{2}(\mathbf{k})]^{2} + 64 \cos^{2} \frac{k_{z}}{2} \times \left(t_{0}^{R} \cos \frac{k_{x}}{2} \cos \frac{k_{y}}{2} \pm t_{y}^{R} \sin \frac{k_{x}}{2} \sin \frac{k_{y}}{2}\right)^{2}.$$
 (27)

The spin degeneracy amounts to the condition $E_+^2 = E_-^2$. This implies with necessity $f_2(\mathbf{k}) = 0$, namely $\mathbf{k} \in \mathcal{K}_{alt}$. If $k_x = 0$ or $k_y = 0$, the last term in the second line of Eq. (27) vanishes. If $k_x = \pi$ or $k_y = \pi$ the first term does. In both cases we indeed have a degeneracy only for $\mathbf{k} \in \mathcal{K}_{alt}$ as expected.

IV. ANOMALOUS HALL EFFECT

The AHE can be understood based on the symmetry considerations. The AHE is finite as \mathcal{T} symmetry is replaced by the combined $\mathcal{T}C_{2z}$ operation. Due to the Onsager relation, $\mathcal{T}C_{2z}$ imposes the restrictions $\hat{\sigma}_{xy} = \hat{\sigma}_{yx}$, $\hat{\sigma}_{xz} = -\hat{\sigma}_{zx}$, and $\hat{\sigma}_{yz} = -\hat{\sigma}_{zy}$ on the conductivity tensor, $\hat{\sigma}$. This implies at most the transport anisotropy in the xy plane in the form of the planar Hall effect, yet no AHE as $\sigma_{xy}^H = (\sigma_{xy} - \sigma_{yx})/2 = 0$. In contrast to \mathcal{T} , the combined $\mathcal{T}C_{2z}$ symmetry is consistent with $\sigma_{xz}^H \neq 0$ and $\sigma_{yz}^H \neq 0$. The unitary τC_{2x} symmetry imposes $\sigma_{xz}^H = 0$ and still allows a finite σ_{yz}^H .

An alternative way to see this is to notice that the ferromagnetic exchange field $\mathbf{B}_F = B_F \hat{x}$ is consistent with the magnetic point group. And the symmetry that allows for a finite \mathbf{B}_F also allows for a finite σ_{yz}^H . It turns out that the weak ferromagnetic component causes a slight enhancement of the AHE (see Appendix C for details).

Physically the finite ferromagnetic exchange field can be thought of as resulting from the canting of the antiferromagnetic magnetization. Such canting must originate from the SOI. Indeed, in this case the spin-only group is inconsistent with a finite \mathbf{B}_F . We expect, therefore, that $\hat{\sigma}_{yz} = 0$ vanishes at zero SOI. Indeed, in this case the additional C_{2z} rotation symmetry applied solely to the orbital motion with spins left untouched enforces $\hat{\sigma}_{yz} = 0$ as the current operator is spin independent. Therefore, a finite SOI is required for AHE. This is unlike the π transition in altermagnet Josephson junctions [24].

The intrinsic contribution to AHE [25,26],

$$\sigma_{ij}^{H} = e^2 \sum_{b\mathbf{k}}^{\prime} \Omega_{ij}^{b}(\mathbf{k}), \tag{28}$$

relates it to the Berry curvature antisymmetric tensor $\Omega_{ij}^b(\mathbf{k}) = -2\mathrm{Im}\langle \partial_{k_i} u_b(\mathbf{k})|\partial_{k_j} u_b(\mathbf{k})\rangle$, where $u_b(\mathbf{k})$ are periodic parts of the Bloch functions, at the band b and momentum \mathbf{k} . At zero temperature the primed summation in Eq. (28) runs over all occupied Bloch states.

Here we limit the consideration to the large exchange field. In this case the upper (u) and lower (l) band doublets are clustered around $+B_{\rm ex}$ and $-B_{\rm ex}$, respectively. The two band doublets belong to the upper (V_u) and lower (V_l) subspaces $V_{u(l)} = \{\phi_A(\mathbf{r})\bar{\chi}_{+(-)}, \phi_B(\mathbf{r})\bar{\chi}_{-(+)}\}$ that approximately decouple.

Projecting the total Hamiltonian Eq. (8) onto $V_{u(l)}$ spaces we obtain two simpler 2×2 effective Hamiltonians:

$$\hat{H}^{u(l)}(\mathbf{k}) = \pm B_{\text{ex}}\rho_0 + f_1(\mathbf{k})\rho_0 - \mathbf{h}^{u(l)}(\mathbf{k}) \cdot \boldsymbol{\rho}, \quad (29)$$

where ρ_0 and ρ are the unit and Pauli pseudospin matrices operating in V_{\pm} , and

$$h_x^{u(l)} = \mp 8t_x^I \sin \frac{k_x}{2} \cos \frac{k_y}{2} \sin \frac{k_z}{2},$$

$$h_y^{u(l)} = -8t_z^I \cos \frac{k_x}{2} \cos \frac{k_y}{2} \cos \frac{k_z}{2},$$

$$h_z^{u(l)} = -2A' f_2(\mathbf{k}),$$
(30)

where we ignore the contribution of $\hat{H}_{B}^{e}(\mathbf{k})$, Eq. (18), for brevity. The x component of \mathbf{h} is opposite at the upper and lower subbands. This ensures that AHE vanishes when all the bands are occupied, and the system is a topologically trivial insulator. Here we consider the metallic regime with the upper (lower) band doublets partially (fully) occupied, respectively. This situation is described by $\hat{H}_{u}(\mathbf{k})$. It gives rise to the two Fermi surfaces split by the spin dependent terms of Eq. (29); see Fig. 3. Even though the spectrum appears as symmetric under the C_{2z} operation, it is not symmetric at finite SOI. Indeed, Eq. (30) shows that $h_{x}^{u(l)}$ flips under this operation. Therefore Bloch states have a different spin dependence at momenta related by C_{2z} .

The integration region in Eq. (28) is contained in between the two split Fermi surfaces arising from $\hat{H}_u(\mathbf{k})$. The straightforward calculation based on Eqs. (29) and (30) yields $\sigma_{xy}^H = 0$, since $\Omega_{xy}^u(-k_x, k_y, k_z) = -\Omega_{xy}^u(k_x, k_y, k_z)$. Similarly, $\sigma_{xz}^H = 0$. The nonzero σ_{yz}^H arises from

$$\Omega_{yz}^{u}(\mathbf{k}) = \frac{A' t_{x}^{I} t_{z}^{I} [2\cos(k_{y}/2)]^{4} (\sin k_{x})^{2}}{|h^{u}(\mathbf{k})|^{3}}.$$
 (31)

We can see that in the limit of the weak SOI, the $k_y=0$ plane hosts the nodal line where $h^u(\mathbf{k})=0$, and Eq. (31) becomes nonanalytic. It is natural to expect this degeneracy to produce the nonanalytic dependence of the AHE on SOI. To clarify this point we consider the set of parameters resulting in a small Fermi surface centered at the Γ point [see Figs. 3(a) and 3(b)]. We take for the diagonal part of the effective Hamiltonian (29) $f_1(\mathbf{k})=E_0\mathbf{k}^2$, which is obtained by setting $A_0=6E_0$ and $A_x=A_y=A_z=-2E_0$ in Eq. (24). We next set the chemical potential counted relative to the bottom of the band at $B_{\rm ex}$, $\mu \ll E_0$. The Fermi momentum becomes $k_F=\sqrt{\mu/E_0}\ll 1$. In the same limit of a small and nearly spherical Fermi surface we approximate

$$h_x^u \approx -2t_x^I k_x k_z, \quad h_y^u \approx -8t_z^I, \quad h_z^u \approx -2A' k_x k_y.$$
 (32)

With these approximations, taking into account the smallness of the Fermi energy, and setting $t_x^I = t_z^I = t$ for the SOI, the Berry curvature simplifies to

$$\Omega_{yz}^{u}(\mathbf{k}) \approx \frac{2A'k_{x}^{2}t^{2}}{\left[A'^{2}k_{x}^{2}k_{y}^{2} + (4t)^{2}\right]^{3/2}}.$$
(33)

To find the asymptotic behavior of σ_{yz}^H in the limit $t \to 0$ note that the Berry curvature is strongly localized in the $k_y=0$ plane [see Fig. 3(c)]. For the fixed k_x and $k_z=\sqrt{k_F^2-k_x^2}$ on a t=0 Fermi surface the k_y integration range $|k_y|<\bar{k}_y$ is fixed by the condition, $E_0\bar{k}_y^2-(A'^2k_x^2\bar{k}_y^2+(4t)^2)^{1/2}<0$. This gives $\bar{k}_y=A'|k_x|/E_0$ not too close to the north pole of the Fermi sphere, $\bar{k}_x<|k_x|< k_F$, with $\bar{k}_x=4\sqrt{|t|E_0}/A'$. Except

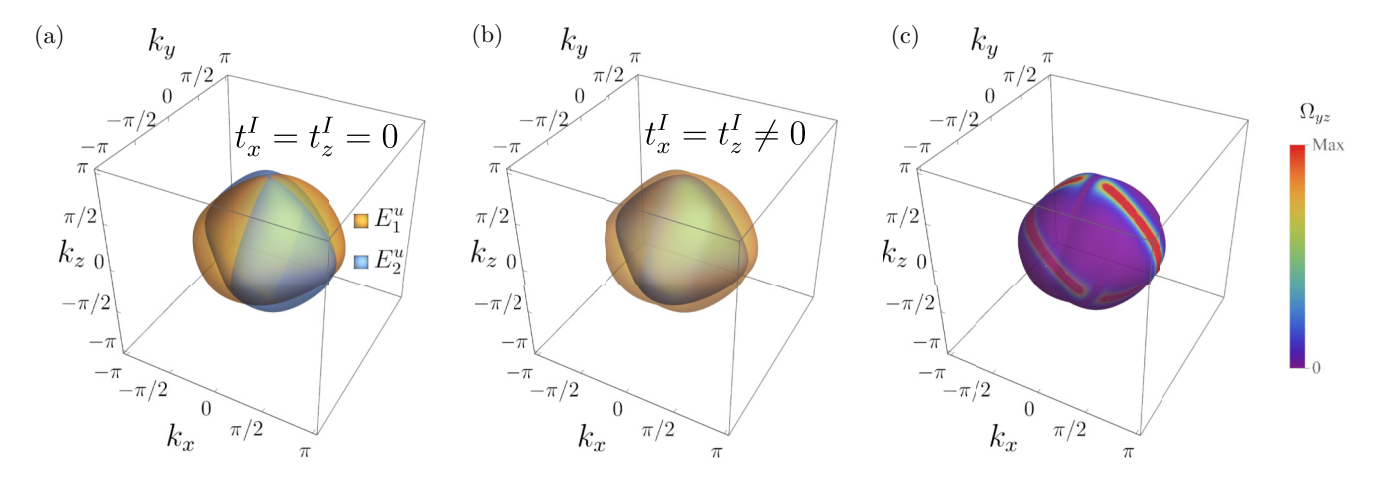


FIG. 3. Fermi surface for the effective Hamiltonian, $\hat{H}_u(\mathbf{k})$, Eq. (29). (a) At zero SOI, $t_x^I = t_z^I$, Eq. (30), the two bands are degenerate at $k_x = 0$ and $k_y = 0$ planes. (b) SOI splits the bands. (c) Berry curvature Ω_{yz}^u , Eq. (31), computed on the external Fermi surface, peaks at the $k_y = 0$ meridian.

for a tiny interval of $|k_x| < 2\bar{k}_x$ the k_y integration of $\Omega^u_{yz}(\mathbf{k})$ converges fast enough to approximate

$$\sigma_{yz}^{H} \approx 4 \int_{-k_{F}}^{-\bar{k}_{x}} \frac{dk_{x}}{2\pi} \int_{\bar{k}^{(1)}}^{\bar{k}_{z}^{(2)}} \frac{dk_{z}}{2\pi} \int_{-\infty}^{\infty} \frac{dk_{y}}{2\pi} \Omega_{yz}^{u}(\mathbf{k}),$$
 (34)

where the factor of 4 accounts for the contributions of the four sectors in the $k_y = 0$ meridian of the Fermi sphere. The straightforward integration over k_y results in

$$\sigma_{yz}^{H} \approx \frac{1}{(2\pi)^3} \int_{-k_F}^{-\bar{k}_x} dk_x |k_x| \int_{\bar{k}_z^{(1)}}^{\bar{k}_z^{(2)}} dk_z.$$
 (35)

In the small t regime, the limits of the k_z integration are set by the energy split $2|\mathbf{h}(\mathbf{k})| \approx 16|t|$ in the $k_y = 0$ plane [see Eq. (32)]. This allows us to perform the k_z integration in Eq. (35), and write

$$\sigma_{yz}^{H} \approx \frac{2|t|}{v_{F}\pi^{3}} \int_{-k_{F}}^{0} dk_{x} \frac{|k_{x}|}{k_{F}} \sqrt{k_{F}^{2} - k_{x}^{2}} = \frac{2|t|k_{F}^{2}}{3v_{F}\pi^{3}},$$
 (36)

where the Fermi velocity $v_F = 2E_0k_F$, and we have set the upper limit of the k_x integration $-\bar{k}_x$ to zero, as the contribution of the region close to the north pole is negligible in this limit.

The numerical coefficient in Eq. (36) depends on the details of the model. The generic feature of Eq. (36) is the nonanalytic linear dependence of the Hall conductivity on the SOI. We have traced its origin to the crossing lines of the Fermi surface(s) with the plane $k_y = 0$. This nonanalyticity is present whenever such crossing occurs, and in this sense is universal. The concentration of the Berry curvature at these crossing(s) expressed via Eq. (33) has been reported for the specific model of SOI in Ref. [1]. The linear in SOI Hall conductivity agrees with the more recent numerical calculations [23]. At the same time the result, Eq. (36), vanishes in the insulating phase as the Fermi surface shrinks. Both trends are illustrated in Fig. 4.

At weak SOI the Hall conductivity, Eq. (36), is independent of the exchange splitting A'. It holds for $t < \mu(A'/E_0)^2$, which may be not too restrictive given that the bandwidth and the Fermi energy μ are of the same order and A' is a few tens of meV based on the DFT of Ref. [27] performed on RuO₂.

V. SUMMARY AND OUTLOOK

In this paper, we have computed the intrinsic anomalous Hall effect of an altermagnet based on the minimal symmetry-constrained tight-binding model. We have studied the collinear altermagnet with and without SOI separately. At finite SOI we have employed an analysis based on the magnetic group symmetry of FeSb₂. We have found the terms that are either even or odd under the $\mathcal T$ symmetry. The terms belonging to the first category agree with the terms obtained in the approaches based on the nonmagnetic space groups [23,28]. The terms odd in $\mathcal T$ describe a combined action of the altermagnetic order parameter and SOI. These require the magnetic group approach.

We next analyzed the zero SOI in the framework of the spin symmetries. In this case we have identified and presented explicitly the symmetry elements including the possibility of acting differently on spin and orbital degrees of freedom. The tight-binding model in this case is considerably more restricted compared to the case of a finite SOI. We note that both the elements of spin-only group as well as the nontrivial

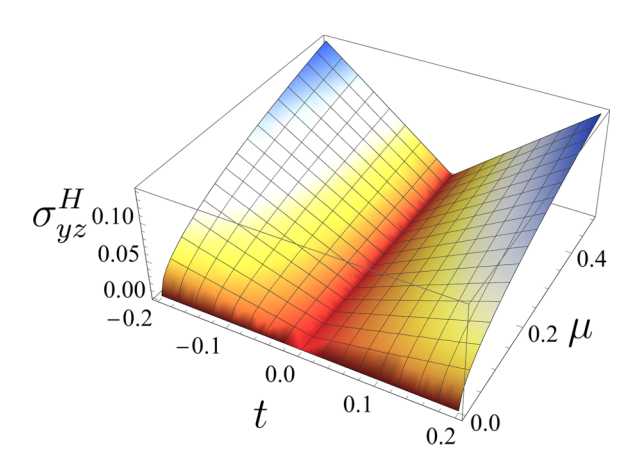


FIG. 4. Hall conductivity, σ_{yz}^H , as given by Eq. (36) as a function of spin-orbit interaction strength, t, and Fermi energy, μ , valid in the regime where the altermagnetic splitting exceeds the SOI spin splitting (arbitrary units).

elements of the spin group are instrumental in restricting the zero SOI model.

Comparison of the models based on magnetic and spin groups respectively allows one to single out the effect of the SOI on the dispersion relation. This would be hard to achieve without having done both types of analysis. We have worked out the band degeneracies based on the Wigner criterion. Usually it is done for the magnetic or nonmagnetic space groups. We have extended this treatment to the spin group in question. The summation over the spin-only elements in this case has to be understood as integration over the continuous spin rotation angle. The tight-binding models in both the finite and zero SOI comply with the general symmetry requirements. And we have used the properly generalized Wigner criterion to benchmark our results.

Here we have focused on $FeSb_2$ material, yet our conclusions are qualitatively similar for other altermagnetic materials such as RuO_2 . According to Refs. [23,28] the SOI has a similar form in two materials. Since the exchange induced splitting has in fact the same form we expect the same results to apply qualitatively to both types of systems.

This paper addresses the intrinsic contribution to AHE. Our model is general, and yet simple enough to serve as a starting point to explore the extrinsic contributions to AHE. One can expect the extrinsic contribution to dominate in the metallic regime where the Fermi energy exceeds the gap due to the SOI as well as the gap induced by the exchange interaction. This task is relegated for future studies.

ACKNOWLEDGMENTS

We would like to thank I. Mazin for invaluable discussions that have been a source of inspiration for the current paper. We are grateful to D. Agterberg and B. Andersen for sharing with us their recent results and pointing our attention to an unusual linear dependence of the Hall conductivity in the SOI. We are grateful to D. Antonenko for providing us with the explanation of their recent work. We thank R. Lifshitz for the discussion of magnetic space groups. We thank I. Gruzberg for the discussion of the time reversal symmetry as acting on degrees of freedom with spin and orbital motion included. We thank M. Smolkin for pointing our attention to universality of the time reversal symmetry, independent on the Lorentz boost magnitude. L.A. and M.K. acknowledge financial support from Israel Science Foundation Grant No. 2665/20. A.L. acknowledges financial support by NSF Grant No. DMR-2203411 and an H. I. Romnes Faculty Fellowship provided by the University of Wisconsin-Madison Office of the Vice Chancellor for Research and Graduate Education with funding from the Wisconsin Alumni Research Foundation.

APPENDIX A: ANTIUNITARY SPIN SYMMETRIES

Here we show that the antiunitary spin symmetries cause no additional degeneracy. The elements of the spin group are listed in Eq. (4). In Sec. II B the unitary half of the spin point group, Eq. (3), has been shown to produce double degeneracy at momenta $\mathbf{k} \in \mathcal{K}_{\text{alt}}$, where \mathcal{K}_{alt} contains four planes: $k_x = 0$, $k_y = 0$, $k_x = \pi$, and $k_y = \pi$.

At a given k, the degeneracy doubles due to the antiunitary operations if at least one of the antiunitary operators in Eq. (4)

TABLE IV. The action of the orbital part of the operations from the list $\{E, \mathcal{P}, m_z, C_{2z}\}$ on the momentum $\mathbf{k} = (k_x, k_y, k_z)$.

E	\mathcal{P}	m_z	C_{2z}
$\overline{(k_x,k_y,-k_z)}$	$(-k_x, -k_y, -k_z)$	$(k_x, k_y, -k_z)$	$(-k_x, -k_y, k_z)$

with \mathcal{T} removed flips **k**. In this case, the extra degeneracy appears in cases (b) and (c):

$$\sum_{g \in \mathcal{G}_{S}^{\prime}}^{\prime} \chi_{\mathbf{k}} \{ [\boldsymbol{\tau}(E||C_{2x})g]^{2} \} = \begin{cases} +[\mathbf{k}]\mathcal{T}^{2} & \text{case (a)} \\ -[\mathbf{k}]\mathcal{T}^{2} & \text{case (b)}. \\ 0 & \text{case (c)} \end{cases}$$
(A1)

The symmorphic unitary operators include the rotations around \hat{y} , $C_y(\varphi)$, by an arbitrary angle, φ . For $\mathbf{k} \notin \mathcal{K}_{\text{alt}}$, $\chi_{\mathbf{k}}[C_y^2(\varphi)] = \exp(\mp i\varphi)$, and for $\mathbf{k} \in \mathcal{K}_{\text{alt}}$, $\chi_{\mathbf{k}}[C_y^2(\varphi)] = 2\cos\varphi$. In both cases $\int_0^{2\pi} d\varphi/(2\pi)\chi_{\mathbf{k}}[C_y^2(\varphi)] = 0$ and therefore the symmorphic operations do not contribute to the sum.

In contrast the nonsymmorphic unitary operations do contribute, since $[C_{2x}C_y(\varphi)]^2 = \bar{E}$, and therefore $\chi_{\mathbf{k}}[C_{2x}C_y(\varphi)]^2 = -1(-2)$ for $\mathbf{k} \notin \mathcal{K}_{alt}$, $(\mathbf{k} \in \mathcal{K}_{alt})$. The action of symmorphic operations on the momentum \mathbf{k} is the same as that of the four operations $\{E, \mathcal{P}, m_z, C_{2z}\}$ given in Table IV.

For a generic \mathbf{k} only the inversion \mathcal{P} contributes to the sum, Eq. (A1), and we have case (a). At the Γ point $\mathbf{k}=0$ all eight unitary operations reverse \mathbf{k} such that $[\mathbf{k}]=8$. And the sum is the product of the point group character -2 and the number of elements contributing +4, and we have case (a) again. Similarly one can show that the case (a) holds throughout the Brillouin zone, and indeed there is no degeneracy caused by the antiunitary operations. So we get no degeneracy doubling due to the antiunitary operations in the case of a given spin symmetry group.

APPENDIX B: SYMMETRY CONSTRAINED HOPPING AMPLITUDES

Here we illustrate the constraints imposed on hopping amplitudes by the magnetic group symmetry (Fig. 5). The most general form of the intersublattice nearest neighbor hopping amplitudes is given in Table II. Here we illustrate the

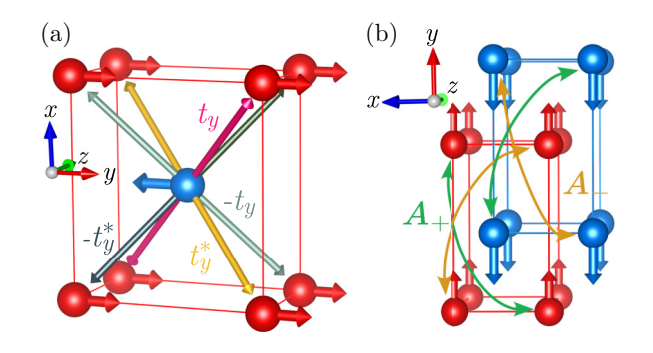


FIG. 5. Amplitudes of hopping between the Fe sites. (a) Intersublattice nearest neighbor hopping amplitudes as summarized in Table II. Only the terms of Eq. (10) $\propto \sigma_y$ are displayed. (b) Intrasublattice next nearest neighbor hopping amplitudes. Only the processes that are distinct for the two sublattices are shown, with the full list of amplitudes given by Table III.

constraints contained in this table in Fig. 5(a). For clarity, we do it just for one out of four types of hopping amplitudes presented in Eq. (10). Namely we consider the $\mu = y$ term of Eq. (10) and show the hopping amplitudes in Fig. 5(a) based on Table II. The remaining three amplitudes can be illustrated in a very similar way based on the same table.

The full information on the intrasublattice hopping amplitudes, $T_{A(B)}(\Delta \mathbf{R})$, over the distance \mathbf{R} is contained in Table III. Here we show the intrasublattice hopping amplitudes important for an altermagnetism in Fig. 5(b).

APPENDIX C: EFFECT OF MAGNETIZATION CANTING ON AHE

Here we study the effect of a weak ferromagnetic component of magnetization on AHE. To clarify this we consider the limit where the exchange field $\mathbf{B}_x = B_x \hat{x}$ is added to the collinear staggered magnetization, such that $B_x \ll B_{\rm ex}$. We do not intend to cover all possible cases, and instead consider the limit of the B_x exceeding the spin splitting at $B_x = 0$.

To find the small correction to AHE in this case we employ the method of the effective Hamiltonian [29]. It is a generalization of the standard perturbation theory to the case of quasidegenerate bands. In our problem we have two quasidegenerate spaces $V_{u(l)} = \{\phi_A(\mathbf{r})\bar{\chi}_{+(-)}, \phi_B(\mathbf{r})\bar{\chi}_{-(+)}\}$ separated by the large exchange energy splitting. In the four-dimensional space spanned by the four states $\{\phi_A(\mathbf{r})\bar{\chi}_+, \phi_B(\mathbf{r})\bar{\chi}_-, \phi_A(\mathbf{r})\bar{\chi}_-, \phi_B(\mathbf{r})\bar{\chi}_+\}$ the Hamiltonian takes the form

$$H = \begin{pmatrix} \hat{H}^{u} & \hat{V}_{ul} \\ \hat{V}_{lu} & \hat{H}^{l} \end{pmatrix}, \tag{C1}$$

where the block diagonal part is specified by Eqs. (29) and (30). For the exchange field $\mathbf{B}_x = B_x \hat{x}$ we have $\hat{V}_{ul} = -i \rho_z$ and $\hat{V}_{lu} = \hat{V}_{ul}^{\dagger}$.

The coupling \hat{V}_{ul} affects the energy levels as well as wave functions of the problem defined for the two-dimensional upper subspace V_u . To the second order in $B_x/B_{\rm ex}$, the energy levels are fixed by the effective Hamiltonian, $\hat{H}^{\rm eff} = \hat{H}^u + \Delta \hat{H}^{\rm eff}$, with

$$\Delta \hat{H}_{ss'}^{\text{eff}} = \frac{1}{2} \sum_{k} {}^{u} \langle s | \hat{V}_{ul} | k \rangle^{l}$$

$$\times \left(\frac{1}{E_{s}^{u} - E_{k}^{l}} + \frac{1}{E_{s'}^{u} - E_{k}^{l}} \right)^{l} \langle k | \hat{V}_{lu} | s' \rangle^{u}, \quad (C2)$$

- [1] L. Šmejkal, R. González-Hernández, T. Jungwirth, and J. Sinova, Crystal time-reversal symmetry breaking and spontaneous Hall effect in collinear antiferromagnets, Sci. Adv. 6, eaaz8809 (2020).
- [2] H. Reichlova *et al.*, Observation of a spontaneous anomalous Hall response in the Mn₅Si₃d-wave altermagnet candidate, Nat. Commun. 15, 4961 (2024).
- [3] I. Turek, Altermagnetism and magnetic groups with pseudoscalar electron spin, Phys. Rev. B 106, 094432 (2022).
- [4] L. Šmejkal, J. Sinova, and T. Jungwirth, Emerging research landscape of altermagnetism, Phys. Rev. X 12, 040501 (2022).

where the states $\hat{H}^{u(l)}|s\rangle^{u(l)} = E_s^{u(l)}|s\rangle^{u(d)}$, s=1,2, diagonalize the two decoupled Hamiltonians. Based on Eq. (29) the energies of the decoupled Hamiltonians read

$$E_{s=1}^{u(l)}(\mathbf{k}) = \pm B_{\text{ex}} + f_1(\mathbf{k}) + |\mathbf{h}^{u(l)}(\mathbf{k})|,$$

$$E_{s=2}^{u(l)}(\mathbf{k}) = \pm B_{\text{ex}} + f_1(\mathbf{k}) - |\mathbf{h}^{u(l)}(\mathbf{k})|.$$
 (C3)

We compute the correction $\Delta H^{\rm eff}$ to the effective Hamiltonian given by Eq. (C2) to the first order in $h/B_{\rm ex}\ll 1$. The first contribution $\Delta H^{\rm eff}_{(a)}$ comes from the expansion of E^l_k , and setting E^s_s to $B_{\rm ex}$. This contribution takes the form, in the original basis V_u ,

$$\Delta \hat{H}_{(a)}^{\text{eff}} = -\frac{B_x^2}{4B_{\text{ex}}^2} \rho_z [\mathbf{h}^l(\mathbf{k}) \cdot \boldsymbol{\rho}] \rho_z. \tag{C4}$$

Additional contribution $\Delta H_{(b)}^{\text{eff}}$ originates from the expansion of $E_{s,s'}^{u(l)}$ in h^u/B_{ex} and setting E_k^l to $-B_{\text{ex}}$ in Eq. (C2):

$$\Delta \hat{H}_{(b)}^{\text{eff}} = -\frac{B_x^2}{4B_{\text{ex}}^2} [\mathbf{h}^u(\mathbf{k}) \cdot \boldsymbol{\rho}]. \tag{C5}$$

Combining Eqs. (C4) and (C5) we obtain for the total correction

$$\Delta \hat{H}^{\text{eff}} = -\frac{B_x^2}{2B_{\text{ex}}^2} h_y^{\mu}(\mathbf{k}) \rho_y. \tag{C6}$$

The result (C6) indicates that the effect of the ferromagnetic magnetization component in the considered limit is the renormalization of the t_z^I interaction amplitude as defined in Eq. (30) to the effective one:

$$t_z^{I,\text{eff}} = t_z^I \left(1 + \frac{B_x^2}{2B_{\text{ex}}^2} \right).$$
 (C7)

Here we focused on the spectrum renormalization. In fact the wave functions also change as a result of the perturbation. This effect can be shown to be negligible in the considered range of parameters.

Equation (C7) indicates that the weak ferromagnetism causes a a slight enhancement of the AHE.

- [5] I. Mazin (The PRX Editors), Editorial: Altermagnetism: A new punch line of fundamental magnetism, Phys. Rev. X 12, 040002 (2022).
- [6] T. A. Maier and S. Okamoto, Weak-coupling theory of neutron scattering as a probe of altermagnetism, Phys. Rev. B 108, L100402 (2023).
- [7] C. R. W. Steward, R. M. Fernandes, and J. Schmalian, Dynamic paramagnon-polarons in altermagnets, Phys. Rev. B 108, 144418 (2023).
- [8] I. I. Mazin, Altermagnetism in MnTe: Origin, predicted manifestations, and routes to detwinning, Phys. Rev. B 107, L100418 (2023).

- [9] R. M. Fernandes, V. S. de Carvalho, T. Birol, and R. G. Pereira, Topological transition from nodal to nodeless Zeeman splitting in altermagnets, Phys. Rev. B 109, 024404 (2024).
- [10] I. I. Mazin, K. Koepernik, M. D. Johannes, R. González-Hernández, and L. Šmejkal, Prediction of unconventional magnetism in doped FeSb₂, Proc. Natl. Acad. Sci. USA 118, e2108924118 (2021).
- [11] S. Hayami and H. Kusunose, Microscopic description of electric and magnetic toroidal multipoles in hybrid orbitals, J. Phys. Soc. Jpn. 87, 033709 (2018).
- [12] S. Hayami, Y. Yanagi, and H. Kusunose, Momentum-dependent spin splitting by collinear antiferromagnetic ordering, J. Phys. Soc. Jpn. 88, 123702 (2019).
- [13] S. Hayami, Y. Yanagi, and H. Kusunose, Bottom-up design of spin-split and reshaped electronic band structures in antiferromagnets without spin-orbit coupling: Procedure on the basis of augmented multipoles, Phys. Rev. B 102, 144441 (2020).
- [14] R. Lifshitz, Magnetic point groups and space groups, in *Encyclopedia of Condensed Matter Physics*, edited by F. Bassani, G. L. Liedl, and P. Wyder (Academic Press, Oxford, 2005), Vol. 3, p. 219.
- [15] K. Momma and F. Izumi, VESTA3 for three-dimensional visualization of crystal, volumetric and morphology data, J. Appl. Crystallogr. 44, 1272 (2011).
- [16] W. F. Brinkman and R. J. Elliott, Theory of spin-space groups, Proc. R. Soc. A 294, 343 (1966).
- [17] D. Litvin and W. Opechowski, Spin groups, Physica 76, 538 (1974).
- [18] L. Šmejkal, J. Sinova, and T. Jungwirth, Beyond conventional ferromagnetism and antiferromagnetism: A phase with nonrelativistic spin and crystal rotation symmetry, Phys. Rev. X 12, 031042 (2022).
- [19] Z. Feng, X. Zhou, L. Šmejkal, L. Wu, Z. Zhu, H. Guo, R. González-Hernández, X. Wang, H. Yan, P. Qin, X. Zhang, H.

- Wu, H. Chen, Z. Meng, L. Liu, Z. Xia, J. Sinova, T. Jungwirth, and Z. Liu, An anomalous Hall effect in altermagnetic ruthenium dioxide, Nat. Electron. 5, 735 (2022).
- [20] S. Hayami and H. Kusunose, Essential role of the anisotropic magnetic dipole in the anomalous Hall effect, Phys. Rev. B 103, L180407 (2021).
- [21] T. Inui, Y. Tanabe, and Y. Onodera, *Group Theory and its Applications in Physics*, Springer Series in Solid-State Sciences (Springer-Verlag, Berlin, 1990), Vol. 78.
- [22] G. Bir and G. Pikus, Symmetry and Strain-induced Effects in Semiconductors, A Halsted Press book (Wiley, Hoboken, NJ, 1974).
- [23] M. Roig, A. Kreisel, Y. Yu, B. M. Andersen, and D. F. Agterberg, Minimal models for altermagnetism, arXiv:2402.15616.
- [24] J. A. Ouassou, A. Brataas, and J. Linder, DC Josephson effect in altermagnets, Phys. Rev. Lett. **131**, 076003 (2023).
- [25] N. A. Sinitsyn, A. H. MacDonald, T. Jungwirth, V. K. Dugaev, and J. Sinova, Anomalous Hall effect in a two-dimensional Dirac band: The link between the Kubo-Streda formula and the semiclassical Boltzmann equation approach, Phys. Rev. B 75, 045315 (2007).
- [26] D. Xiao, M.-C. Chang, and Q. Niu, Berry phase effects on electronic properties, Rev. Mod. Phys. 82, 1959 (2010).
- [27] L. Šmejkal, A. Marmodoro, K.-H. Ahn, R. González-Hernández, I. Turek, S. Mankovsky, H. Ebert, S. W. D'Souza, O. Šipr, J. Sinova, and T. Jungwirth, Chiral magnons in altermagnetic RuO₂, Phys. Rev. Lett. 131, 256703 (2023).
- [28] D. S. Antonenko, R. M. Fernandes, and J. W. F. Venderbos, Mirror Chern bands and Weyl nodal loops in altermagnets, arXiv:2402.10201.
- [29] C. Cohen-Tannoudji, G. Grynberg, and J. Dupont-Roc, *Atom-Photon Interactions: Basic Processes and Applications* (Wiley, New York, 1992).